Simulation of Mass Transfer of Calcium in Concrete by the Lattice Kinetic Scheme for a Binary Miscible Fluid Mixture*

Masato YOSHINO**,***, Toshiro MURAYAMA**, Akihiro MATSUZAKI** and Takashi HITOMI†

** Department of Mechanical Systems Engineering, Shinshu University,
4–17–1, Wakasato, Nagano-shi, Nagano 380–8553, Japan
*** CREST, Japan Science and Technology Agency,
4–1–8, Honcho, Kawaguchi-shi, Saitama 332-0012, Japan
E-mail: masato@shinshu-u.ac.jp
† Technical Research Institute, Obayashi Corporation,
4–640, Shimokiyoto, Kiyose-shi, Tokyo 204–8558, Japan

Abstract

The lattice kinetic scheme (LKS) for a binary miscible fluid mixture was applied to the simulation of the mass transfer of calcium in concrete. Cement paste, a major component of concrete, is a porous medium with a complicated three-dimensional geometry. The structure of the model concrete was selected on the basis of experimental data obtained by high-intensity X-ray computed tomography. The LKS, an improved version of the original lattice Boltzmann method, was used to save computational memory and to maintain numerical stability. First, an unsteady convection–diffusion problem was examined, and the accuracy of the method and the error norms with various lattice resolutions were investigated. Next, the problem of the calcium current in concrete was simulated. Pressure drops in the concrete were calculated for various Reynolds numbers, and the results were compared with those of an empirical equation based on experimental data. Also, velocity fields and concentration profiles were obtained at a pore scale for a structure with inhomogeneous mass diffusivities. These simulations showed that the present method might be useful for predicting calcium leaching in concrete from the microscopic point of view.

Key words : Numerical Simulation, Lattice Boltzmann Method (LBM), Lattice Kinetic Scheme (LKS), Concrete, Porous Structure, X-Ray Computed Tomography (X-Ray CT), Pressure Drops, Pèclet Number

1. Introduction

Concrete is widely used as a fundamental material in construction, and consists of 5–25 mm-sized coarse aggregate (crushed stone), less than 5 mm-sized fine aggregate (sand), and cement paste (cement kneaded with water). The mixture of the fine aggregate and the cement paste is called mortar. Mortar has a porous network structure in which the scale of the pores varies between several nanometers and several micrometers.[1] Because the quality of concrete in prolonged contact with liquids such as seawater or groundwater frequently deteriorates, it is necessary to make precise predictions and estimations of the degree of degradation. The problem is associated with leaching of calcium from the constituent material of concrete. In addition, recent studies[2],[3] have shown that the constituent material of concrete is changed by chemical reactions with ions that penetrate into the material from its surroundings. However, the mechanisms underlying these phenomena remain unclear.

Recently, Saito et al.[4] experimentally studied the transport of calcium in concrete by means of the electrochemical acceleration tests. They also carried out a one-dimensional

mass-transfer simulation by means of a volume-averaged approach, and they verified the appropriateness of the calculated mass diffusivity by comparison with the experimental results. However, it is difficult to perform experimental investigations because of the complexity of the pore structures. Therefore, numerical simulations based on microscopic approaches could be used to investigate transport phenomena of calcium in concrete.

With regard to numerical methods, when conventional Navier–Stokes codes are applied to flows in porous media, we often have trouble with long computational times, poor convergence, and numerical instabilities. Hence, it was desired to develop a new numerical scheme. Since the early 1990s, the lattice Boltzmann method (LBM)[5],[6] has been developed as an alternative and promising numerical scheme for simulating flows of viscous, multicomponent, and multiphase fluids. The advantages of the LBM over standard Navier–Stokes codes are the simplicity of the algorithm in complex systems and the accuracy of the mass and momentum conservations. There have been many studies on transport phenomena in porous media by the LBM. For example, Inamuro et al.[7] and Yoshino and Inamuro[8] investigated viscous flows and binary mass transfer in a porous structure composed of identical spherical bodies for wide range of Reynolds numbers. They also demonstrated the validity and effectiveness of the LBM in such flow problems. Okabe and Blunt[9] performed simulation of flows through porous media reconstructed by using multiple-point statistics[10] for the prediction of the appropriate permeability. Li et al.[11] tackled two-phase fluid flows in three-dimensional porous media to investigate the viscous coupling effect[12] that is characteristic of immiscible two-phase flow. More recently, Seta et al.[13] simulated natural convection in porous media, and they demonstrated the superiority of the LBM to conventional schemes such as the finite-difference method. Yamamoto et al.[14] simulated the accumulation of soot in porous media to examine particle trapping in a diesel particulate filter (a porous medium with a porosity that ranges from about 0.7 to 0.9). Thus, the LBM is expected to be a powerful numerical scheme for simulating mass transfer of calcium in concrete.

To simulate microscopic transport phenomena in concrete, it is essential to obtain information about the pore structure of the material. Landis et al.[15] and Turner et al.[16] have measured actual pore structures by means of X-ray computed tomography (X-ray CT) and micro-CT. Hitomi et al.[17] also conducted nondestructive inspections of pore structures in concrete by means of high-intensity X-ray CT at the Super Photon ring-8 (SPring-8)[18] to extract three-dimensional images of the pores from a sectional view. By making use of the images obtained by these advanced metrologies, we can achieve a clear understanding of microscopic transport phenomena in concrete.

Our aims here are to simulate transport phenomena of calcium in a concrete structure modeled from real images reconstructed by means of X-ray CT and to develop a systematic method for predicting the degradation of concrete as a result of leaching. In particular, we examine how the transfer of calcium is affected by the complicated geometries and convective flows. As a numerical method, the lattice kinetic scheme[19] for a binary miscible fluid mixture is used to save computational memory and to maintain numerical stability at high Pèclet numbers.

2. Numerical Method

As described previously,[20] we use nondimensional variables defined by using a characteristic length L, a characteristic particle speed c, a characteristic time scale $t_0 = L/U$ (where U is a characteristic flow speed), a reference density ρ_0, and a reference mass concentration C_0. We consider a binary miscible fluid mixture composed of water as an incompressible fluid and calcium as a diffuse component. Here, we assume that the mass fraction of calcium is much smaller than that of the fluid; it follows that the concentration of calcium can be regarded as a passive scalar. Moreover, although the calcium exists in the form of ions in the fluid, the electric effect can be neglected because there is no external electric potential.

In the LBM for a binary miscible fluid mixture,[20] two particle velocity distribution

functions, f_i and g_i, are used, where $i = 1, 2, 3, \ldots, N$, where N is the number of particle velocities. The function f_i is used to calculate the fluid density ρ and the fluid velocity $\boldsymbol{u}$; the function g_i is then used to calculate the calcium concentration C. The 15-velocity model ($N = 15$) is used, the velocity vectors of which are given by the following equation:

$$[\boldsymbol{c}_1, \boldsymbol{c}_2, \boldsymbol{c}_3, \boldsymbol{c}_4, \boldsymbol{c}_5, \boldsymbol{c}_6, \boldsymbol{c}_7, \boldsymbol{c}_8, \boldsymbol{c}_9, \boldsymbol{c}_{10}, \boldsymbol{c}_{11}, \boldsymbol{c}_{12}, \boldsymbol{c}_{13}, \boldsymbol{c}_{14}, \boldsymbol{c}_{15}]$$

$$= \begin{bmatrix} 0 & 1 & 0 & -1 & 0 & 0 & 0 & 1 & -1 & -1 & 1 & 1 & -1 & -1 & 1 \\ 0 & 0 & 1 & 0 & -1 & 0 & 0 & 1 & 1 & -1 & -1 & 1 & 1 & -1 & -1 \\ 0 & 0 & 0 & 0 & 0 & 1 & -1 & 1 & 1 & 1 & 1 & -1 & -1 & -1 & -1 \end{bmatrix}. \quad (1)$$

In the LKS, the fluid density ρ, the fluid velocity $\boldsymbol{u}$, and the calcium mass concentration C at a point $\boldsymbol{x}$ and at time t are defined by the following equations:

$$\rho(\boldsymbol{x}, t) = \sum_{i=1}^{15} f_i^{\mathrm{eq}}(\boldsymbol{x} - \boldsymbol{c}_i \Delta x, t - \Delta t), \quad (2)$$

$$\boldsymbol{u}(\boldsymbol{x}, t) = \frac{1}{\rho(\boldsymbol{x}, t)} \sum_{i=1}^{15} \boldsymbol{c}_i f_i^{\mathrm{eq}}(\boldsymbol{x} - \boldsymbol{c}_i \Delta x, t - \Delta t), \quad (3)$$

$$C(\boldsymbol{x}, t) = \sum_{i=1}^{15} g_i(\boldsymbol{x} - \boldsymbol{c}_i \Delta x, t - \Delta t), \quad (4)$$

where

$$f_i^{\mathrm{eq}} = E_i \rho \left[1 + 3 c_{i\alpha} u_\alpha + \frac{9}{2} c_{i\alpha} c_{i\beta} u_\alpha u_\beta - \frac{3}{2} u_\alpha u_\alpha + A \Delta x \left(\frac{\partial u_\beta}{\partial x_\alpha} + \frac{\partial u_\alpha}{\partial x_\beta} \right) c_{i\alpha} c_{i\beta} \right], \quad (5)$$

$$g_i^{\mathrm{eq}} = E_i C (1 + 3 c_{i\alpha} u_\alpha) + E_i B \Delta x \, c_{i\alpha} \frac{\partial C}{\partial x_\alpha}, \quad (6)$$

and

$$\left. \begin{aligned} E_1 &= 2/9, \\ E_2 &= E_3 = E_4 = \cdots = E_7 = 1/9, \\ E_8 &= E_9 = E_{10} = \cdots = E_{15} = 1/72. \end{aligned} \right\} \quad (7)$$

In the above equations, $\alpha, \beta = x, y, z$ (subscripts α and β represent Cartesian coordinates; the summation convention is used henceforth), Δx is a spacing of the cubic lattice, Δt is a time step, and A and B, which are both of $O(1)$, are parameters given below that determine the kinematic viscosity and the mass diffusivity, respectively. Note that the time step Δt is chosen as a time during which the particles travel the lattice spacing; it follows that $\Delta t = \mathrm{Sh} \Delta x$ where $\mathrm{Sh} = U/c$ is the Strouhal number. It has been reported by Inamuro[19] that the LKS is helpful in saving computational memory because there is no need to store the particle velocity distribution functions.

The pressure p is related to the density ρ by the following equation:

$$p = \frac{1}{3} \rho. \quad (8)$$

The kinematic viscosity ν of the fluid and the mass diffusivity D of the calcium in the binary fluid mixture are related to A, B, and Δx as follows:

$$\nu = \left(\frac{1}{6} - \frac{2}{9} A \right) \Delta x, \quad (9)$$

$$D = \left(\frac{1}{6} - \frac{1}{3} B \right) \Delta x. \quad (10)$$

The following finite-difference approximation is used to calculate the first derivative of a scalar variable ψ in Eqs. (5) and (6):

$$\frac{\partial \psi}{\partial x_\alpha} \approx \frac{1}{10 \Delta x} \sum_{i=2}^{15} c_{i\alpha} \psi(\boldsymbol{x} + \boldsymbol{c}_i \Delta x). \quad (11)$$

By applying the asymptotic theory[21],[22] to Eqs. (2)–(6) with appropriate initial and boundary conditions, we find that the velocity for incompressible fluid, the pressure, and the mass concentration of calcium can be calculated with relative errors of $O[(\Delta x)^2]$.[19] In addition, the mass flux of calcium with respect to the mass-average velocity, $\boldsymbol{j}_C$, is given by the following equation:[8],[23]

$$\boldsymbol{j}_C = C(\boldsymbol{u}_C - \boldsymbol{u}), \tag{12}$$

where $\boldsymbol{u}_C$ is defined as

$$\boldsymbol{u}_C = \frac{1}{C} \sum_{i=1}^{15} g_i \boldsymbol{c}_i. \tag{13}$$

3. The Accuracy of the LKS for a Binary Miscible Fluid Mixture

The validity of the numerical method has already been demonstrated for a steady problem of natural convection in a square cavity.[19] Here, a one-dimensional unsteady convection–diffusion problem is calculated to evaluate the accuracy of the method. A rectangular domain of $L_y = L_z = 0.1L_x$ is considered, and a fluid flows with a uniform speed U in the x-direction. A diffuse component is injected from the inlet at time $t = 0$, and the evolution of the concentration is calculated in the domain. At the initial state, a constant concentration $C = C_I$ in the whole domain is assumed. The boundary conditions are $C = C_{in}$ at the inlet ($x = 0$) and $\partial C / \partial x = 0$ at the outlet ($x = L_x$). In the calculation, the concentration at the outlet is given by using the second-order one-sided difference approximation so that the concentration gradient in the x-direction can be equal to zero. Also, at $y = 0$, $y = L_y$, $z = 0$, and $z = L_z$, the periodic boundary condition is used for the fluid velocity, and the normal mass flux of the diffuse component is assumed to be free.

The normalized concentration is defined by the following equation:

$$\Pi = \frac{C - C_I}{C_{in} - C_I}. \tag{14}$$

The governing equation and the initial and boundary conditions are then given as follows:

$$\mathrm{Sh}\frac{\partial \Pi}{\partial t} + U\frac{\partial \Pi}{\partial x} = D\frac{\partial^2 \Pi}{\partial x^2}, \tag{15}$$

$$\left.\begin{array}{lll} t = 0, & 0 \le x \le L_x: & \Pi = 0\,; \\ t > 0, & x = 0: & \Pi = 1\,; \\ t > 0, & x = L_x: & \partial \Pi / \partial x = 0\,, \end{array}\right\} \tag{16}$$

where Sh is the Strouhal number given in Section 2. If L_x is taken as ∞, the exact solution Π^* of this problem is given by the following equation:[24]

$$\Pi^* = \begin{cases} \dfrac{1}{2}\left[1 + \mathrm{erf}\left(\dfrac{Ut/\mathrm{Sh} - x}{\sqrt{4Dt/\mathrm{Sh}}}\right)\right] + \dfrac{1}{2}\exp\left(\dfrac{Ux}{D}\right)\left[1 - \mathrm{erf}\left(\dfrac{Ut/\mathrm{Sh} + x}{\sqrt{4Dt/\mathrm{Sh}}}\right)\right] \\ \qquad\qquad\qquad\qquad\qquad\qquad (\text{for } x < Ut/\mathrm{Sh}) \\[2mm] \dfrac{1}{2}\left[1 - \mathrm{erf}\left(\dfrac{x - Ut/\mathrm{Sh}}{\sqrt{4Dt/\mathrm{Sh}}}\right)\right] + \dfrac{1}{2}\exp\left(\dfrac{Ux}{D}\right)\left[1 - \mathrm{erf}\left(\dfrac{Ut/\mathrm{Sh} + x}{\sqrt{4Dt/\mathrm{Sh}}}\right)\right], \\ \qquad\qquad\qquad\qquad\qquad\qquad (\text{for } x \ge Ut/\mathrm{Sh}) \end{cases} \tag{17}$$

where $\mathrm{erf}(x)$ is the error function given by

$$\mathrm{erf}(x) = \frac{2}{\sqrt{\pi}} \int_0^x e^{-\xi^2}\, d\xi. \tag{18}$$
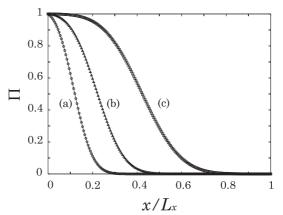
Fig. 1 Normalized concentration profiles in unsteady convection–diffusion problem at various dimensionless times with $\Delta x = 1/200$: (a) ∘, $t^* = 0.1$; (b) △, $t^* = 0.2$; (c) ×, $t^* = 0.4$ ($t^* = tU/L_x$). The solid lines represent the exact solution.

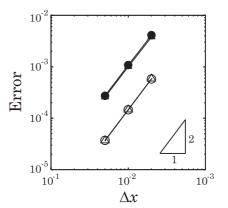Fig. 2 Error norms of unsteady convection–diffusion problem. The symbols ● and ▲ indicate respective Er_1 and Er_2 norms for the present calculation; the symbols ∘ and △ represent the corresponding results for original LBM.

The calculations are conducted by setting L_x to a large value to permit a comparison of the results with the exact solution. The parameters are $L_x = 200\Delta x$, $B = 0.35$, $U = 0.01$, $C_I = 1$, and $C_{in} = 5$. The Pèclet number is then $Pe = UL_x/D = 40$.

First, the concentration profiles at various dimensionless times are shown in Fig. 1. Here the dimensionless time t^* is defined as $t^* = tU/L_x$. The solid lines represent the exact solution obtained from Eq. (17). The calculated results agree well with the exact solution at each time. Next, to determine the convergence rate, the simulation is performed with various lattice resolutions, $L_x = 50\Delta x$, $100\Delta x$, and $200\Delta x$. The fluid velocity U is changed so that the Pèclet number can be kept constant. Figure 2 shows the error norms $Er_1 = \Sigma_x |\Pi - \Pi^*| / \Sigma_x |\Pi^*|$ and $Er_2 = \sqrt{\Sigma_x(\Pi - \Pi^*)^2} / \sqrt{\Sigma_x(\Pi^*)^2}$ at $t^* = 0.2$. The sums are taken over the same 51 nodes in the x-direction regardless of the lattice resolution. The slopes of the convergence are $m_1 = 1.9823$ and $m_2 = 1.9587$ for Er_1 and Er_2, respectively. Hence, the present method is almost a second-order scheme. According to preliminary calculations, the corresponding slopes in the case of the original LBM for a binary miscible fluid mixture are $m_1' = 1.9905$ and $m_2' = 1.9970$. Also, the errors in the present method are about ten times larger than those in the original LBM, as shown in Fig. 2. The main reason is the discretization error in the LKS. Unlike the case of the original LBM, it is necessary that the first derivatives in Eqs. (5) and (6) of the LKS should be discretized by using a certain approximation, although in this problem only $\partial C/\partial x$ is considered because U is constant and a concentration gradient is present in the x-direction only. Therefore, a higher-order difference approximation other than Eq. (11) should be used to obtain more-accurate results with a fixed lattice resolution.
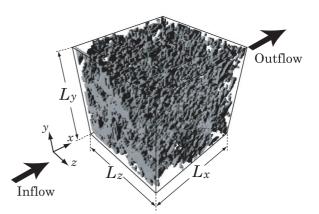
Fig. 3   Three-dimensional concrete structure reconstructed by using data obtained from high-intensity X-ray CT.[17] The degraded and nondegraded regions are represented by the pore phase and the solid phase, respectively.
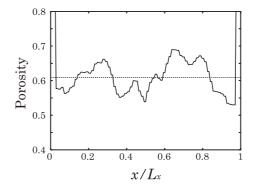

Fig. 4   Porosity distribution on the cross-sections perpendicular to the main stream. $0.029 \leq x/L_x \leq 0.97$ is a porous section.

4. Mass Transfer of Calcium in Concrete

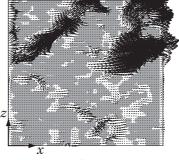### 4.1. The Modeled Concrete Structure

We use a modeled concrete structure reconstructed by using data obtained from high-intensity X-ray CT,[17] as shown in Fig. 3. The microstructure of concrete is composed of a porous part, from which cement hydrate leaches out in the form of an ion, and an unchanged part, where little cement hydrate is degraded. Hereafter, the former is referred to as the degraded region and the latter as the nondegraded region. In Fig. 3, the degraded and nondegraded regions are represented by the pore phase and the solid phase, respectively. The three-dimensional distribution of pores larger than 1μm is obtained by binary processing of images of mortar photographed by high-intensity X-ray CT. By applying these results, we determined the difference between the degraded and nondegraded regions [see Ref. (17) for further details]. Also, the porosity distribution on the cross-sections perpendicular to the main stream is shown in Fig. 4. In the computational domain, $0.029 \leq x/L_x \leq 0.97$ is a porous section representing the concrete model, and the other section is a fully open space. The porosity of the porous section is $\varepsilon = 0.609$.

Although several-nanometer-sized pores are present in the nondegraded region, water seldom passes through these pores because of the high resistance to fluid flow. The transfer rate of calcium in the degraded region is considered to be larger than that in the nondegraded region where many pores are distributed. According to experimental studies,[4],[25] the apparent mass diffusivity in the degraded region is more than ten times that in the nondegraded region, although the difference depends on the size and tortuosity of the pores. Hence, on the basis of these experimental data, the mass diffusivities in the degraded and nondegraded regions are set to different values in the following calculations.

$\longrightarrow 5u_0$

(a)
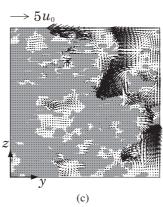
$\longrightarrow 5u_0$

(b)

$\longrightarrow 5u_0$

(c)

Fig. 5   Velocity vectors at $t^* = 4.23$ for Re $= 0.977$: (a) $z/L_z = 0.50$; (b) $y/L_y = 0.50$;
(c) $x/L_x = 0.50$. $t^* = tu_0/d$ and Re $= u_0d/\nu$, where u_0 is the superficial velocity.

4.2. Computational Conditions

The whole domain is divided into a $138 \times 130 \times 130$ cubic lattice. In the initial state, $\rho = 1$, $\boldsymbol{u} = \boldsymbol{0}$, and $C_I = 1$ are assumed in the domain. The boundary conditions are as follows. At the inlet and outlet, the periodic boundary condition with a pressure difference is used for the fluid. The concentrations of calcium are set to $C_{in} = 5$ at the inlet and $\partial C/\partial x = 0$ at the outlet. As in the previous problem, the concentration at the outlet is given by using the second-order one-sided difference approximation so that the concentration gradient in the x-direction can be equal to zero. On the sides of the domain, the no-slip boundary condition is used for the fluid velocity, and the normal mass flux of calcium is fixed at zero. Moreover, at the boundary between the degraded and nondegraded regions, the no-slip boundary condition is used for the fluid velocity. As mentioned above, the fluid velocity in the nondegraded regions is assumed to be zero. The kinematic viscosity of the fluid is $\nu = 0.05\Delta x$, and the mass diffusivities of calcium are $D_1 = 0.1\Delta x$ and $D_0 = 2.86 \times 10^{-3}\Delta x$ in the degraded and nondegraded regions, respectively. Note that the ratio of these mass diffusivities, r $(= D_1/D_0)$, is set to 35 with
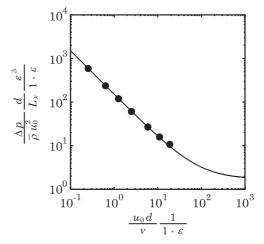
Fig. 6 Pressure drops against modified Reynolds numbers in the concrete structure with a porosity $\varepsilon = 0.609$: ●, the present results; —, the Ergun equation, where $\bar{\rho}$ is the time- and space-averaged fluid density at the inlet.
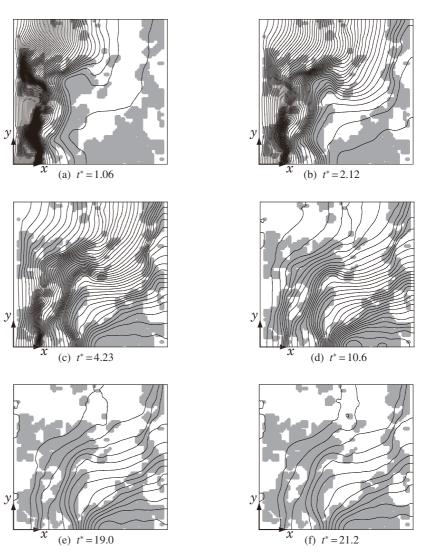

(a) $t^* = 1.06$

(b) $t^* = 2.12$

(c) $t^* = 4.23$

(d) $t^* = 10.6$

(e) $t^* = 19.0$

(f) $t^* = 21.2$

Fig. 7 Temporal variation in concentration contours of calcium on $z/L_z = 0.50$ for $Pe = 0.489$ and $r = 35$ ($t^* = tu_0/d$, $Pe = u_0 d/D_1$, $r = D_1/D_0$). The contour interval is 0.08.

(a) $t^* = 1.06$

(b) $t^* = 2.12$

(c) $t^* = 4.23$

(d) $t^* = 10.6$
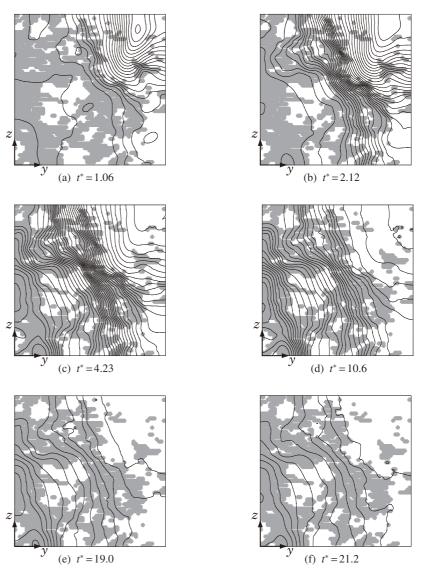
(e) $t^* = 19.0$

(f) $t^* = 21.2$

Fig. 8 Temporal variation in concentration contours of calcium on $x/L_x = 0.50$ for Pe = 0.489 and $r = 35$ ($t^* = tu_0/d$, Pe $= u_0 d/D_1$, $r = D_1/D_0$). The contour interval is 0.08.

reference to the empirical data in Ref. (25) (i.e., it was reported that the value of r ranges from 30 to 40 in the case of mortar where the ratios of water to cement and of sand to cement are 0.4 and 1.5, respectively). In the calculations, the pressure difference Δp between the inlet and outlet is changed so that the Reynolds number Re $= u_0 d/\nu$ and the Pèclet number Pe $= u_0 d/D_1$ become $0.0994 \leq$ Re ≤ 7.38 and $0.0497 \leq$ Pe ≤ 3.69. Here, d is a characteristic length representing the concrete structure and u_0 is the superficial velocity,[23] which is the average velocity that the fluid would have in the channel if the solid phase were absent. In this study, we determine the value of d by comparing the calculated pressure drop with the value given by the Ergun equation[26] at the lowest Reynolds number (Re = 0.0994), as described in the next section: the determined value is $d = 15.2\Delta x$.

Finally, according to Refs. (4) and (17), the characteristic values of the dimensional variables are as follows: fluid velocity, $\tilde{u} \approx 10^{-8}$ m/s; mean pore size, $\tilde{d} \approx 10^{-5}$ m; apparent mass diffusivity of calcium in the degraded region, $\tilde{D}_1 \approx 10^{-12}$ m²/s. The Pèclet number then becomes Pe $= \tilde{u}\tilde{d}/\tilde{D}_1 \approx 10^{-1}$. The present simulation therefore corresponds to actual transport phenomena of calcium in concrete.
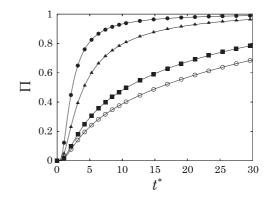
Fig. 9   Temporal variation of normalized concentration of calcium at $(x/L_x, y/L_y, z/L_z) = (0.50, 0.77, 0.50)$ for different Pèclet numbers: ●, Pe = 0.489; ▲, Pe = 0.247; ■, Pe = 0.0497; ○, Pe = 0. $\Pi = (C - C_I)/(C_{in} - C_I)$ and $t^* = tu_0/d$, where u_0 is the superficial velocity for Pe = 0.489.

4.3. Results and Discussion

Figure 5 shows the calculated velocity vectors on three different planes ($z/L_z = 0.50$, $y/L_y = 0.50$, and $x/L_x = 0.50$) at Re = 0.977 after transitional flows. In this figure, the gray and white regions indicate the degraded and nondegraded regions, respectively. It can be seen from (a) and (b) that the fluid tends to go through open spaces. Also, secondary flows can be seen in (c), thus the fluid flows three-dimensionally in the complicated geometry. Figure 6 shows the pressure drops against the modified Reynolds numbers defined as Re′ = Re/(1 − ε). The present results agree well with those of the Ergun equation,[26] which is derived empirically on the basis of experimental data.

Figures 7 and 8 show the temporal variations in the concentration of calcium on the planes $z/L_z = 0.50$ and $x/L_x = 0.50$ for Pe = 0.489. Figure 7 shows that the calcium is transferred in the degraded regions faster than in the nondegraded regions. In Fig. 8, on the plane perpendicular to the main stream, the calculated concentration profiles are distorted in space owing to the convective effect of the secondary flows. As there is little difference between (e) and (f), the flow characteristics and concentration profiles reach their steady state at $t^* \approx 20$, where the dimensionless time is defined as $t^* = tu_0/d$.

Finally, to estimate the convective effects, the temporal variation of the local concentration of calcium is investigated for Pe = 0.0497, 0.247, and 0.489. As an example, the results at a certain position $(x/L_x, y/L_y, z/L_z) = (0.50, 0.77, 0.50)$ are shown in Fig. 9. For comparison, the results for Pe = 0 (without convection) are also plotted in this figure. As the Pèclet number becomes larger, the transfer rate of calcium increases significantly. In particular, the slope of the concentration curve at an early stage for Pe = 0.489 is about four times as large as that for Pe = 0. Moreover, the concentration curve for Pe = 0.489 becomes saturated as early as $t^* \approx 20$. These results show that convective effects associated with seawater or groundwater are of considerable importance in simulations of transport phenomena of calcium in concrete.

5. Concluding Remarks

Numerical simulations of mass transfer of calcium in a three-dimensional concrete structure modeled by high-intensity X-ray CT have been carried out by using the LKS for a binary miscible fluid mixture. The flow characteristics and concentration profiles at a pore scale were obtained by using available physical properties.

Owing to the complicated geometry in concrete, the concentration profiles of calcium were much affected and distorted in three-dimensional space; steep gradients of concentration were observed around complicated boundaries of the degraded and nondegraded regions. Also, convective flows had significant influence on mass transfer of calcium for Pe ≈ 0.5,

which corresponds to a typical case in concrete. With regard to the numerical method, the present approach was found to be useful for the microscopic investigation of mass-transfer problems in complicated geometries. When the LBM for a binary miscible fluid mixture was applied to the same problem, a numerical instability occurred at high Pèclet numbers (results not shown): a higher lattice resolution would have been needed for stable calculation by the original LBM. Consequently, the LKS is superior to the LBM for problems of complex systems such as the one considered here.

Finally, we took no account of leaching of calcium from the constituent materials in the present simulations. A study leading to the development of a numerical method for simulating the leaching of calcium from concrete is required in future work.

Acknowledgments

References

(1) Hitomi, T., Mita, Y. and Takeda, N., Evaluation of Calcium Leaching in Concrete Using High-Intensity X-Ray Computed Tomography (in Japanese), *Proceedings of the Concrete Structure Scenarios, JSMS*, Vol. 5 (2005–10), pp. 223–228.

(2) Sugiyama, T., Shimizu, S. Ritthichauy, W. and Tsuji, Y., Determination of Pore Structure Characteristic of Mortar Using a Steady-State Migration Test (in Japanese), *Journal of Materials, Concrete Structures and Pavements*, Vol. 767, Nos. 5–64 (2004), pp. 227–238.

(3) Hironaga, M., The View and Technology of Concrete for the Disposal of Radio–Active Waste in the Future (in Japanese), *Concrete Journal*, Vol. 37, No. 3 (1999), pp. 3–10.

(4) Saito, H., Tsuji, Y. and Kataoka, H., A Model for Predicting the Leaching Degradation of Cement Hydrate (in Japanese), *Concrete Research and Technology*, Vol. 11, No. 1 (2000), pp. 51–59.

(5) Chen, S. and Doolen, G.D., Lattice Boltzmann Method for Fluid Flows, *Annual Review of Fluid Mechanics*, Vol. 30 (1998), pp. 329–364.

(6) Succi, S., *The Lattice Boltzmann Equation for Fluid Dynamics and Beyond*, (2001), Oxford University Press.

(7) Inamuro, T., Yoshino M. and Ogino, F., Lattice Boltzmann Simulation of Flows in a Three-Dimensional Porous Structure, *International Journal for Numerical Methods in Fluids*, Vol. 29, No. 7 (1999), pp. 737–748.

(8) Yoshino, M. and Inamuro, T., Lattice Boltzmann Simulations for Flow and Heat/Mass Transfer Problems in a Three-Dimensional Porous Structure, *International Journal for Numerical Methods in Fluids*, Vol. 43, No. 2 (2003), pp. 183–198.

(9) Okabe, H. and Blunt, M.J., Prediction of Permeability for Porous Media Reconstructed Using Multiple-Point Statistics, *Physical Review E*, Vol. 70 (2004), 066135.

(10) Caers, J., Geostatistical Reservoir Modelling Using Statistical Pattern Recognition, *Journal of Petroleum Science and Engineering*, Vol. 29, Nos. 3–4 (2001), pp. 177–188.

(11) Li, H., Pan, C. and Miller, C.T., Pore-Scale Investigation of Viscous Coupling Effects for Two-Phase Flow in Porous Media, *Physical Review E*, Vol. 72 (2005), 026705.

(12) Ayub, M. and Bentsen, R.G., Interfacial Viscous Coupling: A Myth or Reality?, *Journal of Petroleum Science and Engineering*, Vol. 23, No. 1 (1999), pp. 13–26.

(13) Seta, T., Takegoshi, E. and Okui, K., Lattice Boltzmann Simulation of Natural Convection in Porous Media, *Mathematics and Computers in Simulation*, Vol. 72, Nos. 2–6 (2006), pp. 195–200.

(14) Yamamoto, K., Satake, S., Yamashita, H., Takada, N. and Misawa, M., Lattice Boltz-

mann Simulation on Porous Structure and Soot Accumulation, *Mathematics and Computers in Simulation*, Vol. 72, Nos. 2–6 (2006), pp. 257–263.

(15) Landis, E.N., Nagy, E.N. and Keane, D.T., Microstructure and Fracture in Three Dimensions, *Engineering Fracture Mechanics*, Vol. 70, Nos. 7–8 (2003), pp. 911–925.

(16) Turner, M.L., Knüfing, L., Arns, C.H., Sakellariou, A., Senden, T.J., Sheppard, A.P., Sok, R.M., Limaye, A., Pinczewski, W.V. and Knackstedt, M.A., Three-Dimensional Imaging of Multiphase Flow in Porous Media, *Physica A*, Vol. 339, Nos. 1–2 (2004), pp. 166–172.

(17) Hitomi, T., Mita, Y., Saito, H. and Takeda, N., Observation of Microscopic Structures of Mortar by X-Ray Computed Tomography in SPring-8 (in Japanese), *Annual Transactions of the Japan Concrete Institute*, Vol. 26, No. 1 (2004), pp. 645–650.

(18) Japan Synchrotron Radiation Research Institute, "Scientific Results: Publications" SPring-8 (online), available from <http://www.spring8.or.jp/en/>, (accessed 2006-10-1).

(19) Inamuro, T., A Lattice Kinetic Scheme for Incompressible Viscous Flows with Heat Transfer, *Philosophical Transactions of the Royal Society A*, Vol. 360, No. 15 (2002), pp. 477–484.

(20) Inamuro, T., Yoshino, M., Inoue, H., Mizuno, R. and Ogino, F., A Lattice Boltzmann Method for a Binary Miscible Fluid Mixture and Its Application to a Heat-Transfer Problem, *Journal of Computational Physics*, Vol. 179, No. 1 (2002), pp. 201–215.

(21) Sone, Y., Asymptotic Theory of Flow of Rarefied Gas over a Smooth Boundary. II, In *Rarefied Gas Dynamics* (ed. Dini, D.), Vol. 2 (1971), Editrice Tenico Scientifica, Pisa, pp. 737–749.

(22) Sone, Y. and Aoki, K., *Molecular Gas Dynamics* (*in Japanese*), (1994), p. 97, Asakura Publishing.

(23) Bird, R.B., Stewart, W.E. and Lightfoot, E.N., *Transport Phenomena*, (1960), p. 500, John Wiley & Sons.

(24) Tanahashi, T., *Introduction to Computational Fluid Dynamics—Convection–Diffusion Equation—* (*in Japanese*), (1996), pp. 224–264, Corona Publishing.

(25) Saito, H., Tajima, T., Fujiwara, A. and Tsuji, Y., Application of Electrochemical Acceleration Test Method to Changes in Cementitious Barrier Performances by Leaching Degradation, *Materials Research Society Symposium Proceedings*, Vol. 506 (1998–4), pp. 449–456.

(26) Ergun, S., Fluid Flow through Packed Columns, *Chemical Engineering Progress*, Vol. 48, No. 93 (1952), pp. 89–94.